Charge Density and Topological Analysis of Pentafluorobenzoic Acid

Ansgar Bach,*,† Dieter Lentz,‡ and Peter Luger†

Institut für Chemie/Kristallographie, Freie Universität Berlin, Takustrasse 6, D-14195 Berlin, Germany, and Institut für Chemie/Anorganische und Analytische Chemie, Freie Universität Berlin, Fabeckstrasse 34-36, D-14195 Berlin, Germany

Received: December 31, 2000; In Final Form: May 29, 2001

A charge density study of crystalline pentafluorobenzoic acid has been carried out using high-resolution X-ray diffraction data collected at 110 K. Two multipole refinement models based on the rigid-pseudoatom formalism were used for topological analysis, and the results were compared to those of theoretical calculations for the isolated molecule. In an analysis of the topological parameters at the bond critical points, the discussion focuses on the C−F bond, the hydrogen bond, and intramolecular and intermolecular weak F···O and F···F′ interactions. Moreover, the geometrical distribution of the nonbonded valence shell charge concentrations was studied at oxygen and fluorine atoms on the basis of experimental data.

Introduction

The electronic charge density $\rho(\mathbf{r})$ of a chemical structure is physically observable, in contrast to the wave function in Schrödinger's equation. The charge density can be deduced from a high-resolution X-ray diffraction experiment[1] at low temperature. According to Bader's theory of atoms in molecules (AIM),[2] developed by a quantum chemical approach, the topological analysis of $\rho(\mathbf{r})$ allows a partitioning of a structure into submolecular regions (atoms or functional groups) and provides a quantitative description of bonds, nonbonded interactions, structure, and reactivity.

The highly polar C−F bond has been the subject of several charge density studies including $F_4SC(CH_3)CF_3$,[3] difluorobenzene derivates,[4] a difluorocubane derivate,[5] and 7-fluoro-4-styrylcoumarin,[6] but only in two cases (*p*-fluoromandelic acid[7] and 1,1-difluoroallene[8]) were quantitative topological data derived, and those data showed large discrepancies between theoretical and experimental results. Because interesting structural studies on low-melting fluorinated hydrocarbons were done[9,10] and are in progress[11] for a charge density study, the very stable and properly crystallizing pentafluorobenzoic acid (PFBA) was to serve as a reference in this field. Results of the charge density distribution and its topological analysis are reported on the basis of an X-ray data set at $d_{min} = 0.40$ Å ($(\sin\theta_{max})\lambda^{-1} = 1.26$ Å^{-1}) resolution measured at 110 K and for comparison on a B3LYP density functional ab initio calculation using the 6-311++G(3df,3pd) basis set.

Experimental and Computational Methods

X-ray data from high-quality crystal (grown by slow evaporation from the saturated solution in an 80:20 mixture of ethanol/2-propanol) were collected on a Bruker SMART CCD-diffractometer. Cooling to 110 K was achieved by an N_2 gas stream device. The measurement strategy was planned with ASTRO,[12] the data collection was monitored with SMART,[13] and the frames were integrated and corrected with the SAINT[13] and SADABS[14] programs. Further details of the experimental X-ray work are summarized in Table 1. For the subsequent theoretical and multipole refinement calculations, the starting atomic parameters were obtained by direct methods[15] and were identical with published data from conventional X-ray analysis with spherical atom refinement.[16]

TABLE 1: Crystal Data and Experimental Conditions

empirical formula	$C_7F_5O_2H$
formula weight	424.16 g/mol
measurement temperature	110 K
diffractometer	SMART-CCD (BRUKER)
sample−detector distance	2.90 cm
radiation type, wavelength	Mo Kα, 0.7107 Å (graphite monochromator)
time per frame (high-order refln)	124 s
time per frame (low-order refln)	30 s
increment $\Delta\omega$	0.3
crystal system, space group	triclinic, $P\bar{1}$
lattice constants	$a = 6.1979(2)$, $b = 7.7748(2)$, $c = 8.0055(2)$ Å $\alpha = 114.89(1)°$, $\beta = 97.49(1)°$, $\gamma = 92.02(1)°$
unit cell volume	345.18(3) Å^3
Z	2
density (calculated)	2.04 g cm^{-3}
absorption coefficient	$\mu = 0.23$ mm^{-1}
transmission factors min/max	0.90/0.97
$F(000)$	208
range for data collection	$2.0° \le 2\theta \le 126.5°$
index ranges	$-15 \le h \le 15$, $-19 \le k \le 18$, $-20 \le l \le 18$
resolution/completeness/ redundancy	7.17−0.69 Å/100%/4−5.3-fold 0.69−0.50 Å/100%/2.8−3.3-fold 0.50−0.45 Å/95%/2.1-fold 0.45−0.40 Å/80%/1.1-fold
reflections collected	31 153
reflections collected > 3σ	16 689
independent reflections	10 483
independent reflections > 3σ	5970
R(int)	5.3%
$R(\sigma)$	2.5%

A full geometry optimization of the isolated molecule of PFBA was performed on the density functional B3LYP level with the basis set 6-311++G(3df,3pd) using the GAUSSIAN

* To whom correspondence should be addressed. E-mail: xbach@chemie.fu-berlin.de. Tel: 0049-30-838 56785. Fax: 0049-30-838 53464.
† Institut für Chemie/Kristallographie.
‡ Institut für Chemie/Anorganische und Analytische Chemie.

10.1021/jp004626n CCC: $20.00
Published on Web 07/14/2001

TABLE 2: Summary of Refinement Results of Different Models

	spherical	M1	M2
$R(F)$ [%]	3.7	2.3	2.4
$R_w(F)$ [%]	3.9	2.1	2.2
GOF	2.3	1.3	1.3
N_{ref}/N_v	45	15	25

98 program package.[17] The results were used for a topological analysis which was done with the AIMPAC program.[18]

The multipole refinements based on the Hansen−Coppens formalism[19] were carried out with the least-squares subprogram XDLSM of XD, a computer program package for refinement and analysis of experimental electron densities in crystals.[20] Input geometry was taken from the spherical refinement.

The quantity $\sum_H w_H(|F_o(H)| - k|F_c(H)|)^2$ was minimized using the statistical weight $w_H = [\sigma(F_o(H))]^{-2}$, where F_o and F_c are the observed and calculated structure factors. Only those structure factors were included which met the criterion $F_o(H) > 3\sigma(F_o(H))$. The multipole model was expanded to the hexadecapole level ($l = 4$) for the heavy atoms (C, O, F) and up to the quadrupolar level ($l = 2$) for the hydrogen atom of the carboxyl group. The O(2)−H(1) distance was fixed to 1.015 Å, as suggested by neutron data.[21] For each atom in a chemically different position (C(sp^2)-*ortho*, C(sp^2)-*meta*, C(sp^2)-*para*, C(OO), F-*ortho*, F-*meta*, F-*para*, O(C=O), O(O−H), and H), individual radial screening parameters (κ) were assigned and refined. The refined κ parameters show a slight expansion for fluorine (κ range, 0.98−0.99) and oxygen (κ range, 0.97−0.99) and a contraction for carbon (κ range, 1.01−1.04) and hydrogen ($\kappa = 1.14$ in model M1 and $\kappa = 1.17$ in model M2). Two density models (M1 and M2) were applied in the multipole refinements of experimental data and compared to the theoretical model obtained from the B3LYP/6−311++G(3df,3pd) optimization. Model M1 applies no atomic site symmetry. Model M2 applies cylindrical symmetry for all fluorine atoms and *mm*2 symmetry for the carbons and O(1) resulting in restrictions for the indices (l, m) of the spherical harmonics. From the statistical figures (Table 2), it is evident that the more restricted model M2 fit the data as well as model M1. Although the ratio of observations to variables increases by more than 60%, the residuals remain practically unchanged.

An additional refinement of the second expansion−contraction parameter κ'[19,20] was done for the atoms C, O, and F on the basis of model M2. The κ' values show slight expansion for F and O (κ' for F, 0.99; κ' for O(1), 0.97; and κ' for O(2), 0.99) and a slight contraction for carbon (κ' for C, 1.01). But this refinement did not change the structural and topological parameters significantly.

Results and Discussion

PFBA crystallizes in space group $P\bar{1}$ with two molecules in the unit cell which are connected by the hydrogen bond O(2)−H(1)···O(1) via the crystallographic inversion center. The distance H(1)···O(1) is 1.642 Å and indicates a very strong hydrogen bond. The molecular structure and crystal packing were well discussed before.[16] The resulting geometrical parameters of the multipole refinements (for both models) agree in the range of 0.02 Å for the lengths and in the range of 0.2° for the angles with the conventional refinement of Benghiat and Leiserowitz.[16] The agreement in bond lengths [see Table 4] between the present experiment and theory is in the range of 0.005 Å except for the two C−O bonds involved in the hydrogen bonds, an interaction which is not considered in the theoretical

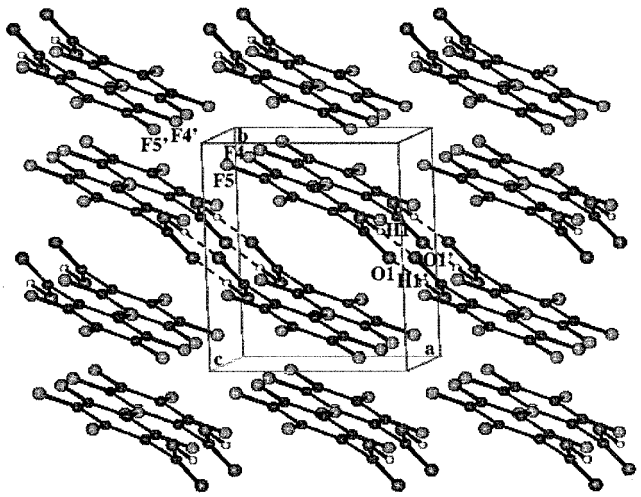

Figure 1. Crystal packing of PFBA.

model. But the most obvious difference between theoretical and experimental geometry is observed in the inclination between the phenyl ring and the carboxyl group planes. The theoretical model predicts a torsion angle C(6)−C(1)−C(7)−O(2) of 41.8° for the isolated molecule, whereas experimental data in the crystal give a significantly smaller value of 29.8(8)°, which is very likely also a result of the parallel stacking of the phenyl groups or of the formation of the strong hydrogen bonds or of the combination of both influences [Figure 1]. The small inclination causes short nonbonding intramolecular F···O contacts in the experimental geometry. The intramolecular distances, F(6)···O(2) = 2.6456(5) Å and F(2)···O(1) = 2.6965(5) Å, are well below the F···O van der Waals contact of 2.99 Å.[22] Theoretical calculation leads to the distances F(6)···O(2) = 2.7533 Å and F(2)···O(1) = 2.8452 Å. Short intermolecular fluorine−fluorine contacts are observed for F(4)···F(4)′ ($2 - x$, $-y$, $1 - z$) with 2.6269(7) Å and F(5)−F(5)′ ($2 - x$, $-y$, $-z$) with 2.6277(6) Å, which are less than the sum of van der Waals radii (2.94 Å).[22]

The experimental static deformation density $\Delta\rho(\mathbf{r})$ (SDD), defined as the difference between the atom-centered multipole density and the charge distribution of a hypothetical spherical promolecular density ρ(pro), was found to be in good agreement with the corresponding theoretical distribution. Figure 2 compares experimental and theoretical static deformation density maps in the two main molecular planes. The SDD maps show qualitatively charge accumulations in the nonpolar covalent bonds (C−C), in the polar bonds (C−F, C−O) and in the nonbonded valence shell regions around the oxygen and fluorine atoms. In the directions of polar bonds, there is a lack of charge accumulation near the more electronegative atom (with lone pairs) because of the molecular spherical distributions at these atoms which contribute too much density in the bond direction for the spherical model in ρ(pro).[23,24]

For both multipole models, the same trend for the monopole charges is observed [Table 3]. The carbon atoms, C(4) in the para position and C(2) and C(6) in the ortho positions, have a higher positive monopole charge (around 3.7) than C(3) and C(5) in the meta positions (4.0) have. In substitution reactions, nucleophilic reagents prefer the para and ortho positions because the mesomeric para- and orthochinoide resonance forms are stabilized.[25] The atom O(1) of the carboxyl group has a distinctly higher negative monopole charge (6.5) than has O(2) (6.1). The hydrogen atom, as expected, carries a positive monopole charge.

Figure 3 shows relief plots of the negative Laplacian $-\nabla^2\rho(\mathbf{r})$ of the total density based on the experimental data (model M2)

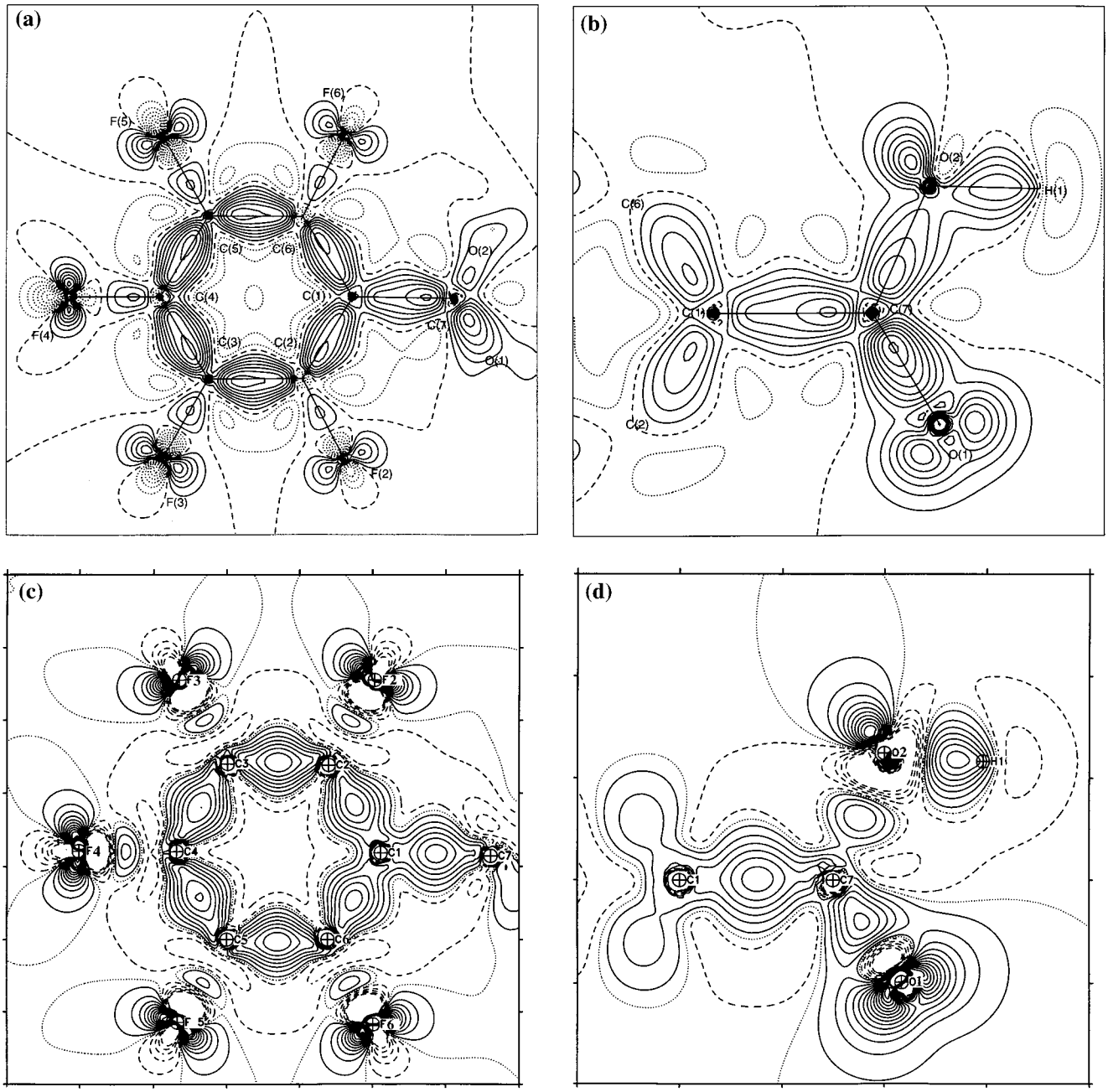

Figure 2. Experimental SDD maps in the planes of the phenyl group (a) and of the carboxyl group (b) and corresponding theoretical maps ((c) and (d), respectively) from the B3LYP optimization. The contour intervals are at 0.1 e/Å^3, zero, and negative corresponding to the lines, dotted lines, and dashed lines, respectively.

for the two molecular planes, the phenyl ring (Figure 3a) and the carboxyl group (Figure 3b). The distributions of the *valence shell charge concentrations* (VSCC) differ. Around the carbon atoms, three bonded VSCCs were found. For the nonpolar C−C bonds, the VSCC maxima in bond direction form a symmetric saddle between the bonds. The polar bonds C−O and C−F show asymmetric saddles in the relief plots. For the oxygen and fluorine atoms also, nonbonded VSCC (nbVSCC) maxima were located. These nbVSCCs are discussed later.

The quantitative results of the topological analysis are summarized in Table 4. For polar C−F bonds, there are significant differences found for the values of the Laplacian between the experimental models (M1, M2) and the theoretical model. In the multipole models based on experimental data, the negative Laplacian at the (3,−1) bond critical points of the C−F bonds ranges from 18.1(1) to 25.7(1) e/Å^5, which is typical

TABLE 3: Experimental Monopol Charges

atom	charge/model	atom	charge/model
C(1)	3.81(7)/M1	F(2)	7.20(2)/M1
	3.83(5)/M2		7.19(2)/M2
C(2)	3.71(5)/M1	F(3)	7.24(2)/M1
	3.71(4)/M2		7.23(2)/M2
C(3)	4.00(5)/M1	F(4)	7.09(3)/M1
	4.00(5)/M2		7.08(2)/M2
C(4)	3.66(6)/M1	F(5)	7.24(2)/M1
	3.67(5)/M2		7.23(2)/M2
C(5)	4.00(5)/M1	F(6)	7.20(2)/M1
	4.00(5)/M2		7.19(2)/M2
C(6)	3.71(5)/M1	O(1)	6.51(4)/M1
	3.71(4)/M2		6.49(4)/M2
C(7)	3.83(6)/M1	O(2)	6.12(6)/M1
	3.81(5)/M2		6.17(5)/M2
H(1)	0.68(5)/M1		
	0.67(5)/M2		

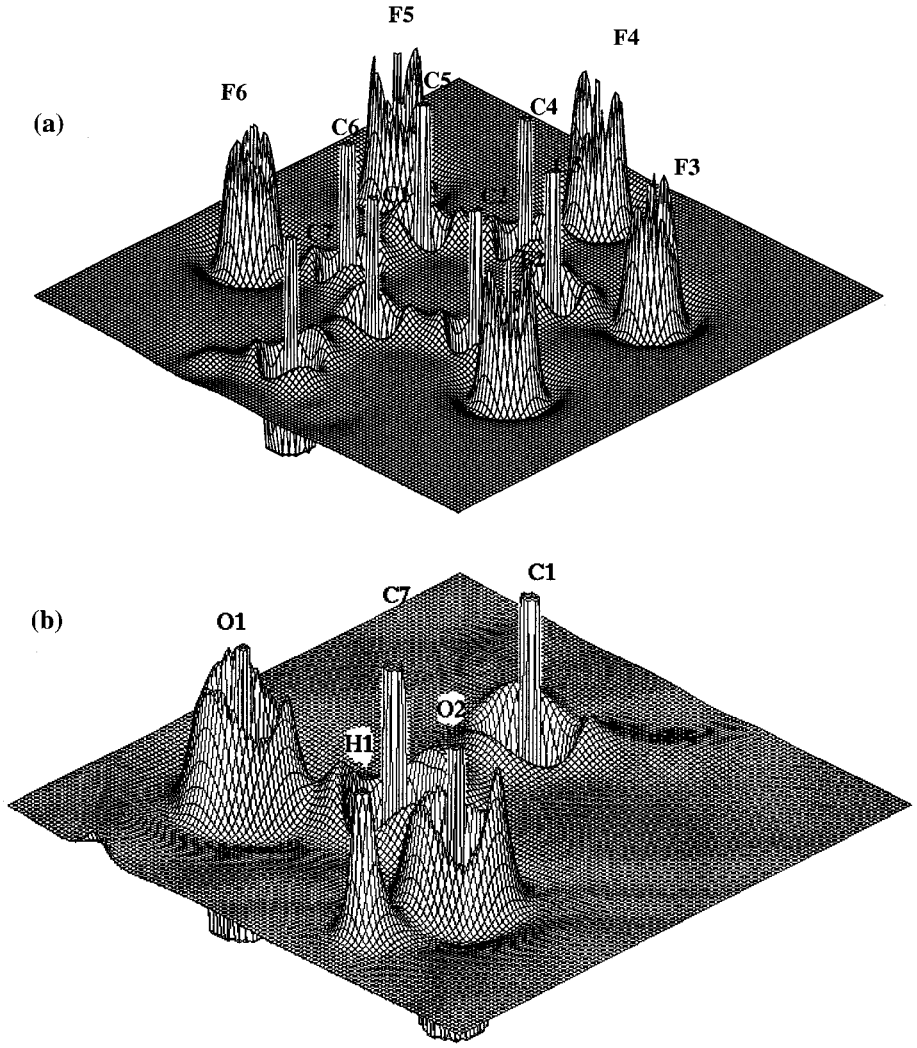

Figure 3. Relief plots giving the negative Laplacian $-\nabla^2\rho(\mathbf{r})$ of the total experimental density for the plane of the phenyl ring (a) and of the carboxyl group (b).

for covalent bonds. In earlier studies, $-\nabla^2\rho(\mathbf{r})$ of C(sp^2)−F bonds was found to be 15(4) e/Å^5 for *p*-fluoromandelic acid[7] and 10.2(4) e/Å^5 for 1,1-difluoroallene.[8] The theoretically calculated Laplacian for C−F bonds is close to zero, ranging from −0.49 to 0.18 e/Å^5; the theoretical densities at these bond critical points range from 1.86 to 1.90 e/Å^3, which is about 90−95% of the experimental density (2.0−2.1 e/Å^3). Noticeable differences between experiment and theory are also seen for the C−O bonds; however, they are involved in the hydrogen bonding in the crystal, which is not considered in the theoretical calculation of the isolated molecule. These topological differences between experimental and theoretical charge densities particularly for the Laplacian at the bond critical points for polar bonds have been observed before.[7,8,26] According to Coppens et al.,[26] the main origin of these discrepancies is attributed to the nature of the radial functions in the experimental multipole model and not to the differences between the isolated molecule and the crystal or to the use of different basis sets. The radial functions contribute to the location of the bond critical points in the topological analysis. The different behavior of $\rho(\mathbf{r})$ and $\nabla^2\rho(\mathbf{r})$ in the polar C−F and the nonpolar C−C bond regions based on the experimental data as well as on theoretical calculations is displayed in Figure 4. For the nonpolar bond, the location of a (3,−1) critical point is in a rather flat minimum along the bond where the Laplacian does not change very much, but along the polar C−F bond, the Laplacian undergoes a change of sign just between the experimental and theoretical (3,−1) critical points.

For the nonpolar bonds C−C and C−H, there is a very good agreement beween the results of experimental and theoretical topological analyses.

(3,−1) Critical points were found not only for chemical bonds but also for other interactions: the intramolecular contacts between F(2)···O(1) and F(6)···O(2), the intermolecular interaction for the hydrogen bond −O(1)···H(1), and the short fluorine−fluorine contacts as F(4)−F(4)′ and F(5)−F(5)′. The (3,−1) critical points for C−F···O and F···F′ interactions were not expected, and these interactions were assumed to be very weak.[16] The paths of these interactions are congruent with the shortest connection lines. The charge density at the intramolecular F···O (3,−1) critical points is 0.08 e/Å^3, that at the intermolecular F···F′ (3,−1) critical points is about 0.06 e/Å^3, and the negative Laplacian is found to be around 1.6 e/Å^5 for F···O and 2.3 e/Å^5 for F···F′. By the topological analysis based on experimental data, these interactions are decribed quantitatively. The theoretical topological analysis leads to no (3,−1) critical points for the intramolecular F···O paths. In theory, the F···O distances are longer than those that resulted from diffraction data. Very likely, these effects are related to the differences in the torsion angle C(6)−C(1)−C(7)−O(2) between the theoretical model for an isolated molecule and the crystal geometry. The intermolecular F···F interactions seem to be of

TABLE 4: Topological Parameters at the (3,−1) Critical Points and at the (3,+1) Ring Critical Points[c]

bond	lengths [Å]	d_1[a] [Å]	$\rho(\mathbf{r})$ [e/Å^3]	$-\nabla^2\rho(\mathbf{r})$ [e/Å^5]	ϵ[b]
C(2)−F(2)	1.3298(4)	0.503	2.01(3)	21.8(1)	0.18
(ortho)	1.3291(5)	0.509	2.02(2)	21.7(1)	0.17
	1.3285	0.44	1.89	0.49	0.02
C(6)−F(6)	1.3322(5)	0.507	2.01(1)	21.6(1)	0.18
(ortho)	1.3325(5)	0.506	2.00(1)	21.5(1)	0.17
	1.3312	0.44	1.88	0.47	0.02
C(3)−F(3)	1.3290(5)	0.508	2.10(3)	25.2(1)	0.19
(meta)	1.3291(5)	0.509	2.12(3)	25.7(1)	0.15
	1.3301	0.44	1.88	−0.18	0.05
C(5)−F(5)	1.3294(5)	0.508	2.10(4)	24.9(1)	0.20
(meta)	1.3296(5)	0.509	2.12(4)	25.73(6)	0.15
	1.3306	0.44	1.86	−0.17	0.05
C(4)−F(4)	1.3188(5)	0.528	2.11(4)	18.1(1)	0.04
(para)	1.3189(5)	0.527	2.12(2)	18.5(2)	0.02
	1.3262	0.44	1.90	−0.16	0.02
C(1)−C(2)	1.4012(4)	0.682	2.06(3)	18.6(1)	0.39
	1.4017(4)	0.691	2.06(2)	18.74(8)	0.37
	1.3955	0.67	2.13	22.00	0.28
C(2)−C(3)	1.3877(4)	0.664	2.21(2)	20.74(8)	0.43
	1.3871(4)	0.679	2.22(1)	21.29(5)	0.42
	1.3865	0.69	2.21	23.93	0.36
C(3)−C(4)	1.3889(5)	0.712	2.16(2)	20.41(9)	0.46
	1.3894(4)	0.708	2.20(2)	21.15(6)	0.43
	1.3882	0.70	2.20	23.73	0.36
C(4)−C(5)	1.3886(5)	0.671	2.24(3)	22.0(1)	0.44
	1.3878(5)	0.680	2.21(2)	21.29(7)	0.43
	1.3879	0.69	2.21	23.76	0.36
C(5)−C(6)	1.3873(4)	0.713	2.17(1)	20.36(5)	0.45
	1.3878(4)	0.709	2.22(1)	21.25(2)	0.42
	1.3876	0.69	2.22	23.88	0.36
C(6)−C(1)	1.3996(5)	0.724	2.08(3)	20.7(1)	0.34
	1.3995(4)	0.709	2.07(1)	19.09(7)	0.37
	1.3945	0.68	2.13	21.96	0.28
C(1)−C(7)	1.4945(5)	0.721	1.74(3)	11.90(8)	0.17
	1.4946(4)	0.721	1.74(2)	10.9(1)	0.13
	1.4972	0.74	1.79	16.50	0.10
O(1)−C(7)	1.2238(5)	0.769	3.04(5)	38.6(3)	0.14
	1.2239(5)	0.773	3.04(4)	39.1(2)	0.13
	1.1995	0.59	2.99	13.09	0.14
O(2)−C(7)	1.3088(5)	0.755	2.49(4)	21.8(1)	0.13
	1.3086(5)	0.775	2.44(3)	24.1(1)	0.12
	1.3455	0.53	2.12	17.55	0.06
O(2)−H(1)	1.015	0.755	2.25(8)	50.0(8)	0.03
	1.015	0.752	2.27(5)	44.2(5)	0.03
	0.970	0.78	2.48	69.67	0.01
F(2)···O(1)	2.6972(7)	1.313	0.084(2)	1.604(2)	0.56
	2.6964(5)	1.316	0.085(2)	1.622(2)	0.91
	2.8452				
F(6)···O(2)	2.6463(7)	1.304	0.087(2)	1.687(2)	0.52
	2.6456(6)	1.302	0.087(3)	1.695(2)	0.79
	2.7533				
F(4)···F(4)	2.6269(8)	1.319	0.058(1)	1.233(3)	0.01
$(2-x, -y, 1-z)$	2.6370(4)	1.319	0.059(1)	1.253(2)	0.01
F(5)···F(5)	2.6277(6)	1.314	0.067(1)	1.41(1)	0.00
$(2-x, -y, -z)$	2.6274(4)	1.314	0.068(1)	1.433(1)	0.00
O(1)···H(1)	1.6422	1.314	0.31(8)	1.4(1)	0.02
$(-x, 1-y, -z)$	1.6422	1.331	0.31(1)	1.84(9)	0.01
ring CP1			0.11(1)	2.5(1)	
(aromat)			0.11(1)	2.6(1)	
			0.14	3.49	
ring CP2			0.02(1)	0.8(1)	
(bridge of dimers)			0.02(1)	0.8(1)	

[a] d_1 is the distance from the first atom of a bond to the critical point (3,−1). [b] The ellipticity, ϵ, is $\lambda_1/(\lambda_2 - 1)$, where λ_1 and λ_2 are the two negative curvatures of $\rho(r)$ at the (3,−1) critical point. [c] First Row of Data Refers to Model M1, the Second Row to M2, and the Third to the Theoretical Model.

energetic disadvantage. But the crystal packing, including the stacking of phenyl groups and the formation of hydrogen bonds, is very likely of more energetic advantage than the disadvantage of short F···F contacts. Periodic Hartree−Fock calculations may later contribute to a better understanding of the intermolecular influences. Figure 1 shows how F(4)/F(5) and F(4)′/F(5)′ on one side and the carboxylic acid groups on the other side face each other in a kind of head-to-head or tail-to-tail arrangement, respectively, in the packing. The experimental density at the (3,−1) critical points for these interactions is about 3%−4% of that of a covalent bond. This indicates a very weak interaction when compared to the hydrogen bond in which the electron density at the (3,−1) critical point is higher. The topological parameters for the intermolecular hydrogen bond are comparable to those found in other compounds, e.g., in amino acids and peptides.[27−29] The experimental density, ρ(r), of 0.31 e/Å^3 at the (3,−1) critical point of the hydrogen bond is about 15% of that in a covalent bond.

TABLE 5: Topological Indices at the Maxima of Nonbonded VSCCs

no. of nbVSCC	atom	atom−nbVSCC [Å]	$\rho(\mathbf{r})$[a] [e/Å^3]	$-\nabla^2\rho(\mathbf{r})$[a] [e/Å^5]
1	O(1)	0.343	6.18	127.84
2	O(1)	0.343	6.18	127.85
1	O(2)	0.340	6.25	144.75
2	O(2)	0.344	6.06	110.62
1	F(2)	0.299	9.92	217.11
2	F(2)	0.299	9.94	217.12
3	F(2)	0.299	9.93	217.12
1	F(3)	0.298	10.12	227.71
2	F(3)	0.298	10.08	227.70
3	F(3)	0.298	10.09	227.71
1	F(4)	0.297	10.18	224.97
2	F(4)	0.297	9.79	220.86
3	F(4)	0.297	10.16	224.97
1	F(5)	0.298	10.09	227.71
2	F(5)	0.298	10.10	227.72
3	F(5)	0.298	10.10	227.72
1	F(6)	0.299	9.95	217.11
2	F(6)	0.299	9.94	217.12
3	F(6)	0.299	9.93	217.12

[a] The program routine does not include the calculation of standard uncertainties for these quantities.

A good agreement between the results by experiment and those by theory is also observed at the (3,+1) ring critical point for the phenyl group. In addition to the (3,+1) ring critical point which was expected for the phenyl ring, another (3,+1) ring critical point corresponding to the hydrogen-bonded carboxylic acid dimer was found. At the latter one, there are significantly smaller values for the charge density (0.02 e/Å^3) and for the negative Laplacian (0.8 e/Å^5) when compared to those at the ring critical point of the phenyl group with values of 1.1 e/Å^3 and 2.5 e/Å^5, respectively.

To get a quantitative description of the nonbonded VSCCs, an analytical Newton−Raphson search for the maxima in the negative Laplacian, $-\nabla^2\rho(\mathbf{r})$, of the total density based on the experimental data (model M2) was done for the valence shell sphere around the fluorine and the oxygen atoms. The topological parameters, $\rho(\mathbf{r})$ and $-\nabla^2\rho(\mathbf{r})$, are given in Table 5. For every oxygen atom, two nbVSCCs were localized as (3,−3) critical points in the negative Laplacian, while three critical points of this type were obtained at each fluorine atom. The positions of the nbVSCCs are displayed in Figure 5. Although the nbVSCCs cannot be equated with the lone pairs of two electrons of opposite spin, the maxima are oriented in a geometric range which is predicted by the valence-shell electron-pair repulsion (VSEPR) model.[30,31] For O(1), the coplanarity of the nbVSCCs with the carboxyl plane and the angle of 126° between both nbVSCCs and C(7)−O(1) support a trigonal planar

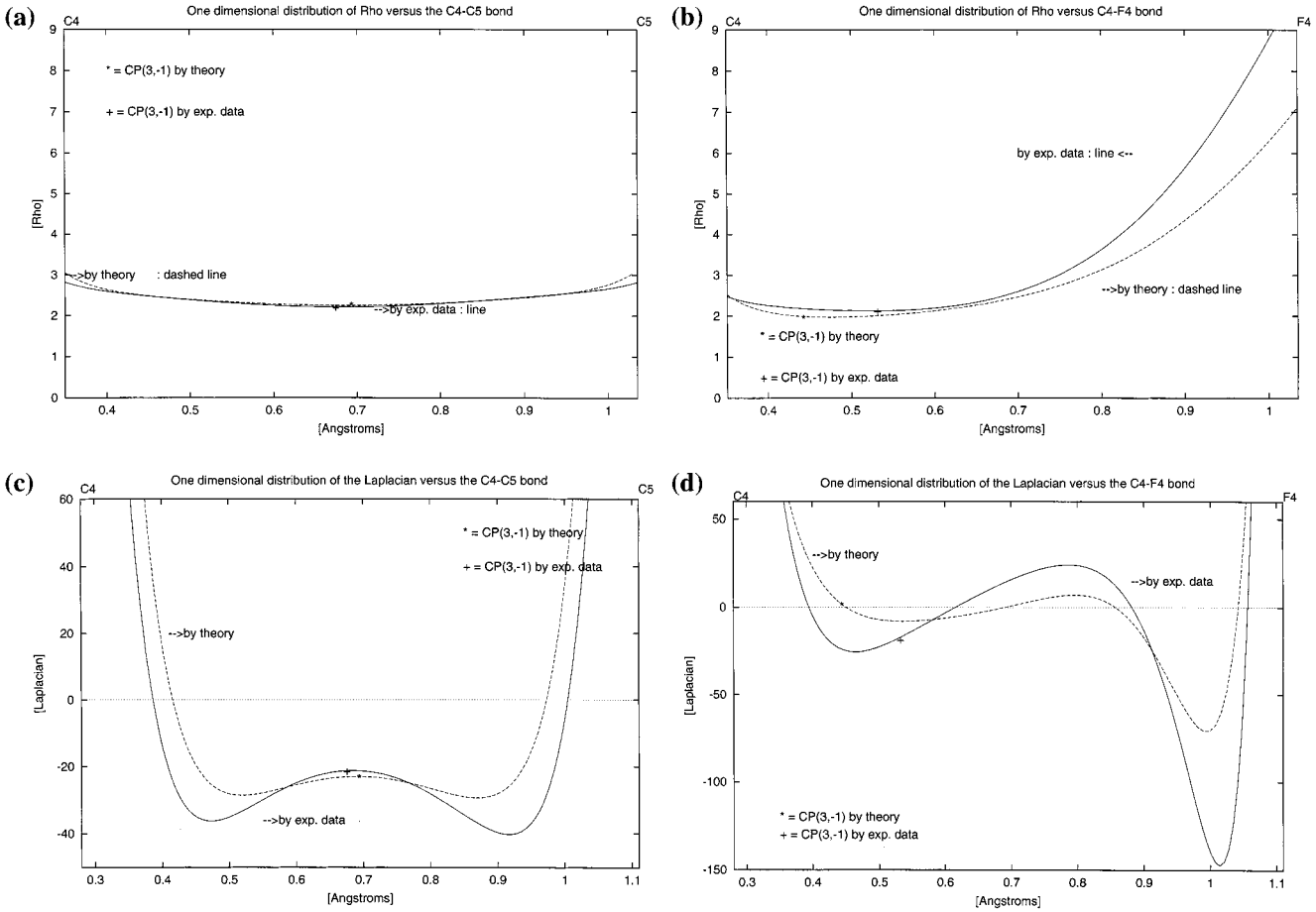

Figure 4. One-dimensional experimental and theoretical distributions of $\rho(\mathbf{r})$ [e/Å^3] (*y*-axis in Figure 4a,b) and of $\nabla^2\rho(\mathbf{r})$ [e/Å^5] (*y*-axis in Figure 4c,d) versus the C4−C5 and C(4)−F(4) bonds (*x*-axes, [Å]). Experimental and theoretical bond critical points are marked with plus mark and asterisk, respectively.

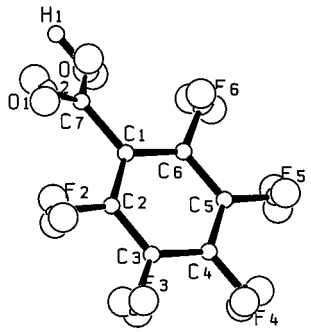

Figure 5. Located maxima of nonbonded valence shell charge concentrations (big circles) around fluorine and oxygen atoms in the molecular structure of PFBA.

geometry. The distance O(1)−nbVSCC is 0.34 Å, and the distance nbVSCC−nbVSCC is 0.54 Å. For O(2), the angles between the nbVSCCs and the bonds to adjacent atoms range from 91° to 121°, forming a distorted tetrahedron. The distance O(2)−nbVSCC is 0.34 Å, and between the nbVSCCs, it is 0.54 Å.

For each fluorine atom, three maxima of nbVSCCs form a triangle in a plane which is perpendicular to the plane of the phenyl group. The distances between a fluorine atom and its nbVSCCs range from 0.297 to 0.299 Å. The angles between two nbVSCCs and the corresponding fluorine atom range from 93° to 133°, indicating a distorted tetrahedral geometry. The distortion may be also related to the F···O and F···F interactions. The distances between two nbVSCCs at one fluorine atom range from 0.44 to 0.54 Å.

The molecular dipole moment of PFBA was calculated for the two multipole refinement models and by theory (B3LYP/6-311++G(3df,3pd)) for the isolated molecule in the optimized geometry as well as in the crystal geometry. On the basis of the diffraction data, an enhancement of the electrostatic moments of molecules in the crystals due to an induced polarization by the crystal field and hydrogen bonds had to be expected.[32] The molecular dipole moment is by theory for an isolated molecule in the optimized geometry 1.7 D and for an isolated molecule in the crystal geometry 1.9 D. In the crystal, it is increased to 4.2(5) D for model M1 and to 3.8(4) D for model M2. These large differences are attributed also by Coppens et al.[26] to a lack of intrinsic physical constraints in the multipole refinement.

The electrostatic potential was calculated using the method of Su and Coppens[33] on the basis of the experimental model M2 and is displayed in Figure 6. This calculation considers the hydrogen-bonded dimer extracted from the crystal and still containing the polarization effects induced by intermolecular interactions, like the hydrogen bonds. The isosurface representation of a hydrogen-bonded dimer of PFBA shows a region of negative potential around the atom O(1) of the carboxyl group and the fluorine atoms in the ortho and the meta position (F(2), F(3), F(5), F(6)). A region of positive potential is found around the flourine F(4) in the para position and around the hydroxyl group which is involved in the hydrogen bond.

Conclusion

This charge density study of pentafluorobenzoic acid focused on the polar C(sp^2)−F bond, the hydrogen bond, and the

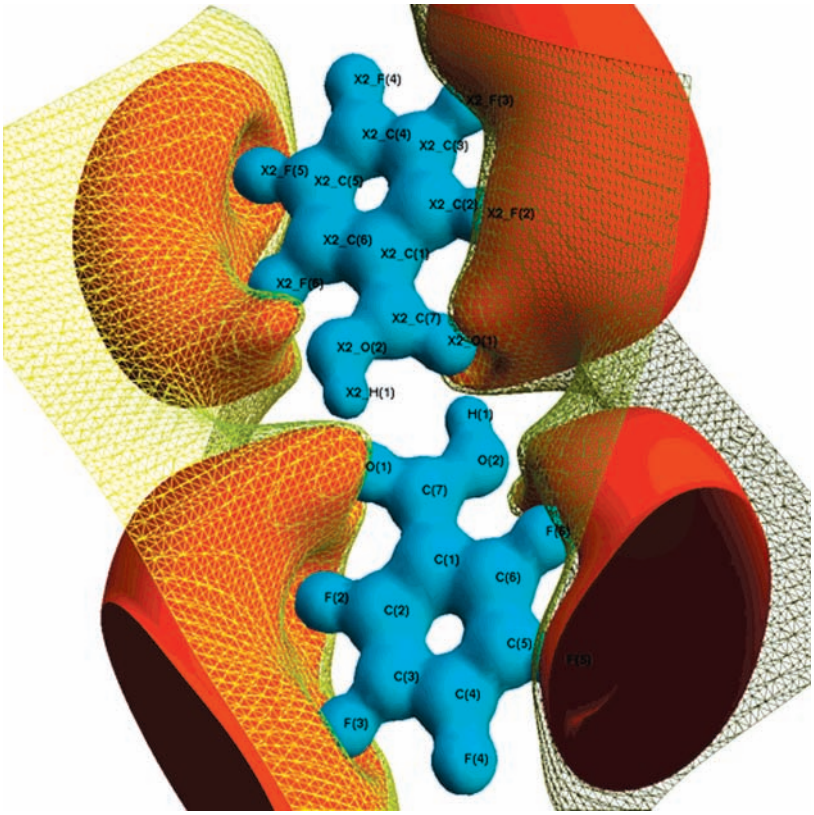

Figure 6. Three-dimensional electrostatic potential based on experimental data for the hydrogen-bonded dimer of PFBA. Three isopotential surfaces are shown: blue 0.50, red −0.03, and net 0.00 e/Å. Symmetry-generated atoms are marked with the X2_ prefix.

nonbonding interactions F···F and F···O, including a topological analysis of the experimental and theoretical electron density to yield quantitative data. The parameters of the topological analysis are in good agreement with other studies on the C−F bond, which used other experimental conditions and other basis sets for theoretical ab initio calculations. This agreement includes the discrepancies between the theoretical and experimental Laplacian for the C−F bond. The theoretical Laplacian changes its sign close to the (3,−1) bond critical points of C−F bonds and is therefore about zero, which means that the C−F interaction is dominated by a concentration of charge density in the atomic basins. The experimental Laplacian is negative, which is typical for a covalent bond which is dominated by a concentration of density toward the bond path. (3,−1) Critical points bearing very low charge densities were also found for weak intramolecular F···O and intermolecular F···F′ interactions and for the hydrogen bond. The F···F′ and F···O interactions are weak when compared to hydrogen bonds. The energetic disadvantage of repulsive F···F′ and F···O interactions is smaller than the energetic advantage of the sum of all crystal field effects including the stacking of the phenyl groups and the formation of hydrogen bonds.

Two (3,+1) ring critical points were found, one for the aromatic ring ($\rho(\mathbf{r}) = 0.11$ e/Å^3) and one for the bridge by hydrogen bonds building a dimer ($\rho(\mathbf{r}) = 0.02$ e/Å^3).

Moreover, searches in the atomic valence shell sphere of the experimental Laplacian at the F and O atoms were carried out in order to locate maxima of nonbonded valence shell charge concentrations (nbVSCCs). The maxima are orientated in a way which is in the range of a geometry predicted by the VSEPR model.

Discrepancies between the experimental and theoretical Laplacian at the bond critical points of the C−F bond and uncertainties in calculating a physical property like the molecular dipole moment are remaining, but it was shown that charge density studies with topological analysis are very worthwhile to get quantitative parameters for characterizing bonds and nonbonding interactions from experimental data.

Acknowledgment. This research was supported by the Deutsche Forschungsgemeinschaft (DFG, Az. Lu222/18-3) and the Fond der Chemischen Industrie.

Supporting Information Available: Tables of multipole population parameters, residual maps, mean-square displacement amplitudes, and X-ray crystallographic data file in CIF format. This material is available free of charge via the Internet at http://pubs.acs.org.

References and Notes

(1) Coppens, P. *X-ray Charge Densities and Chemical Bonding*; Oxford University Press: New York, 1997.

(2) Bader, R. F. W. *Atoms in Molecules—A Quantum Theory*; Clarendon Press: Oxford, U.K., 1990. See, also: Souhasso, M.; Blessing, R. H. *Appl. Crystallogr.* **1999**, *32*, 210.

(3) Buschmann, J.; Koritsánszky, T.; Kuschel, R.; Luger, P.; Seppelt, K. *J. Am. Chem. Soc.* **1991**, *113*, 233.

(4) Kubota, M.; Ohba, S. *Acta Crystallogr.* **1992**, *B48*, 849.

(5) Irngartinger, H.; Shack, S. *J. Am. Chem. Soc.* **1998**, *120*, 5818.

(6) Mallinson, P. R.; Barr, G.; Coles, S. J.; Guru Row, T. N.; MacNicol, D. D.; Teat, S. J.; Wozniak, K. *J. Synchrotron Radiat.* **2000**, *7*, 160.

(7) Larsen, S.; Flensburg, C.; Bengacted, H. S.; Sørenson, H. O. *Acta Crystallogr.* **1999**, *AS55*, 38.

(8) Buschmann, J.; Koritsánszky, T.; Lentz, D.; Luger, P.; Nickelt, N.; Willemsen, S. *Z. Kristallogr.* **2000**, *215*, 487.

(9) Abdo, B. T.; Alberts, I. L.; Attfield, C. J.; Banks, R. E.; Blake, A. J.; Brain, P. T.; Cox, A. P.; Pulham, C. R.; Rankin, D. W.; Robertson, H. E.; Murtagh, V.; Heppeler, A.; Morrison, C. *J. Am. Chem. Soc.* **1996**, *118*, 209.

(10) Bach, A.; Buschmann, J.; Lentz, D.; Luger, P. *Z. Kristallogr.* **2000**, *215*, 518.

(11) Bach, A.; Buschmann, J.; Lentz, D.; Luger, P.; Nickelt, N.; Willemsen, S. *Abstracts of the 17th International Symposium—Fluorine Chemistry*; University of Durham: Durham, U.K., 2000.

(12) *Siemens: ASTRO*; Siemens Analytical X-Ray Intruments Inc.: Madison, WI, 1995.

(13) *Siemens: SMART and SAINT. Data Collection and Processing Software for the SMART System*; Siemens Analytical X-Ray Intruments Inc.: Madison, WI, 1995.

(14) Blessing, R. H. *Acta Crystallogr.* **1995**, *A51*, 33.

(15) Sheldrick, G. M. *SHELXS-93: Program for Crystal Structure Solution*; Institut für Anorganische Chemie der Universität Göttingen: Göttingen, Germany, 1993.

(16) Benghiat, V.; Leiserowitz, L. *J. Chem. Soc., Perkin Trans. 2* **1972**, 1778.

(17) Frisch, M. J.; Trucks, G. W.; Schlegel, H. B.; Scuseria, G. E.; Robb, M. A.; Cheeseman, J. R.; Zakrzewski, V. G.; Montgomery, J. A., Jr.; Stratmann, R. E.; Burant, J. C.; Dapprich, S.; Millam, J. M.; Daniels, A. D.; Kudin, K. N.; Strain, M. C.; Farkas, O.; Tomasi, J.; Barone, V.; Cossi, M.; Cammi, R.; Mennucci, B.; Pomelli, C.; Adamo, C.; Clifford, S.; Ochterski, J.; Petersson, G. A.; Ayala, P. Y.; Cui, Q.; Morokuma, K.; Malick, D. K.; Rabuck, A. D.; Raghavachari, K.; Foresman, J. B.; Cioslowski, J.; Ortiz, J. V.; Stefanov, B. B.; Liu, G.; Liashenko, A.; Piskorz, P.; Komaromi, I.; Gomperts, R.; Martin, R. L.; Fox, D. J.; Keith, T.; Al-Laham, M. A.; Peng, C. Y.; Nanayakkara, A.; Gonzalez, C.; Challacombe, M.; Gill, P. M. W.; Johnson, B. G.; Chen, W.; Wong, M. W.; Andres, J. L.; Head-Gordon, M.; Replogle, E. S.; Pople, J. A. *Gaussian 98*, revision A.7; Gaussian, Inc.: Pittsburgh, PA, 1998.

(18) Cheeseman, J.; Keith, T.; Bader, R. F. W. *AIMPAC program package*; McMaster University: Hamilton, Ontario, Canada, 1992.

(19) Hansen, N. K.; Coppens, P. *Acta Crystallogr.* **1978**, *A34*, 909.

(20) Koritsánszky, T.; Howard, S.; Richter, T.; Su, Z.; Mallinson, P. R.; Hansen, N. K. *XD—a Computer Program Package for Multipole Refinement and Analysis of Electron Densities*; Freie Universitaet Berlin: Berlin, Germany, 1995.

(21) *International Tables For Crystallography*; Wilson, A. J. C., Ed.; Kluwer Academic Publishers: Dordrecht, Boston, London, 1992; Vol. C.

(22) Bondi, A. *J. Phys. Chem.* **1964**, *68*, 441.

(23) Dunitz, J. D.; Schweizer, W. B.; Seiler, P. *Helv. Chim. Acta* **1983**, *66*, 123.

(24) Seiler, P.; Schweizer, W. B.; Dunitz, J. D. *Acta Crystallogr.* **1984**, *B40*, 319.

(25) Hudlický, M. *Chemistry of Organic Fluorine Compounds*; Ellis Harwood: Chichester, U.K. 1976.

(26) Volkov, A.; Abramov, Y.; Coppens, P.; Gatti, C. *Acta Crystallogr.* **2000**, *A56*, 332.

(27) Dittrich, B.; Flaig, R.; Koritsánszky, T.; Krane, H.-G.; Morgenroth, W.; Luger, P. *Chem.—Eur. J.* **2000**, *14*, 2582.

(28) Flaig, R.; Koritsánszky, T.; Zobel, D.; Luger, P. *J. Am. Chem. Soc.* **1998**, *120*, 2227.

(29) Flaig, R. Neue Experimentelle Methoden der Ladungsdichtebestimmung. Doctoral Thesis, Institut für Chemie, Freie Universität Berlin, Berlin, Germany, 2000.

(30) Gillespie, R. J.; Nyholm, R. S. *Q. Rev., Chem. Soc.* **1957**, *11*, 239.

(31) Gillespie, R. J. *Molecular Geometry*; Van Nostrand Reinhold: London, 1972.

(32) Abramov Y., Volkov A. V.; Coppens, P. *Chem. Phys. Lett.* **1999**, *311*, 81.

(33) Su, Z. W.; Coppens, P. *Acta Crystallogr.* **1992**, *A48*, 188.